J|A|C|S
ARTICLES

Published on Web 05/29/2009

Ion-Induced Formation of Charge-Transfer States in Conjugated Polyelectrolytes

Justin M. Hodgkiss,*,†,§ Guoli Tu,‡ Sebastian Albert-Seifried,† Wilhelm T. S. Huck,‡ and Richard H. Friend*,†

Cavendish Laboratory, Department of Physics, University of Cambridge, CB3 0HE, U.K., and Melville Laboratory for Polymer Synthesis, Department of Chemistry, University of Cambridge, CB2 1EW, U.K.

Received March 20, 2009; E-mail: justin.hodgkiss@vuw.ac.nz; rhf10@cam.ac.uk

Abstract: We use time-resolved optical spectroscopy to demonstrate that the luminescence quenching observed when ions are incorporated in films of conjugated polymers can be explained by the formation of charge-transfer (CT) states that are stabilized by the Coulomb field of ions. Our investigation is focused on a conjugated polyelectrolyte (CPE) derived from F8BT (poly(9,9′-dioctylfluorene-*alt*-benzothiadiazole)). The statistical copolymer contains tetra-alkyl ammonium moieties and BF_4^- counteranions attached to a moderate (∼7%) density of polymer alkyl side chains, providing a film morphology comparable to F8BT but with ions distributed on the length scale of exciton diffusion. The ionic substituents have little influence over the polymers electronic absorption and emission properties in solution, however photoluminescence (PL) quantum efficiency (∼6%) is considerably lower for the polyelectrolyte compared with F8BT (∼60%) in thin films. Time-resolved PL spectroscopy reveals that the primary exciton lifetime is shortened in the polyelectrolyte and a red-shifted CT emission peak with a longer lifetime emerges. Transient absorption spectroscopy of thin films enables us to detect CT states that persist beyond the primary decay and are found to be immobile. The PL intensity of the partially ionic film is found to increase with decreasing temperature, consistent with thermally activated exciton hopping ($E_{act} = 28$ meV) prior to formation of CT states at ionic regions. We suggest that ion-induced stabilization of CT states is a general phenomenon in CPEs, which raises the possibility that ions might be arranged to direct the flow of excitons toward charge-separating interfaces in polymer photovoltaic devices.

Introduction

Semiconducting polymers make remarkably effective substitutes for conventional inorganic semiconductors in a range of optoelectronic devices including light emitting diodes (LEDs),[1,2] photovoltaic (PV) diodes,[3−5] field effect transistors (FETs),[6,7] and lasers.[8,9] Conjugated polymers offer considerable material advantages over inorganic semiconductors including chemically tunable optoelectronic properties and low-temperature, solution-based processing suitable for printed electronics. However, their additional functional potential has not been so widely recognized until recently. One functional advantage offered by conjugated polymers is their capacity to employ both electronic and ionic charge carriers in device operation. Whereas solid-state inorganic semiconductors are typically impermeable and unstable toward extrinsic ions, ion transport is at the heart of energy conversion[10,11] and signaling[12] in the soft functional materials found in nature.

Benefits of using ionic charge carriers have been demonstrated in polymer FETs,[13,14] dye-sensitized solar cells,[15−17] and

† Department of Physics.
‡ Department of Chemistry.
§ Current address: School of Chemical and Physical Sciences, Victoria University of Wellington, P.O. Box 600, Wellington, New Zealand.

(1) Burroughs, J. H.; Bradley, D. D. C.; Brown, A. R; Marks, R. N.; Mackay, K.; Friend, R. H.; Burns, P. L.; Holmes, A. B *Nature* **1990**, *347*, 539–541.
(2) Friend, R. H; Gymer, R. W.; Holmes, A. B.; Burroughes, J. H.; Marks, R. N.; Taliani, C.; Bradley, D. D. C.; Dos Santos, D. A.; Bredas, J. L.; Logdlund, M.; Salaneck, W. R. *Nature* **1999**, *397*, 121–128.
(3) Halls, J. J. M.; Walsh, C. A.; Greenham, N. C.; Marseglia, E. A.; Friend, R. H.; Moratti, S. C.; Holmes, A. B. *Nature* **1995**, *376*, 498–500.
(4) Yu, G.; Gao, J.; Hummelen, J. C.; Wudl, F.; Heeger, A. J. *Science* **1995**, *270*, 1789–1791.
(5) Hoppe, H; Sariciftci, N. S. *J. Mat. Res.* **2004**, *19*, 1924–1945.
(6) Garnier, F.; Hajlaoui, R.; Yassar, A.; Srivastava, P. *Science* **1994**, *265*, 1684–1686.
(7) Sirringhaus, H. *Adv. Mater.* **2005**, *17*, 2411–2425.
(8) Tessler, N.; Denton, G. J.; Friend, R. H. *Nature* **1996**, *382*, 695–697.
(9) McGehee, M. D.; Diaz-Garcia, M. A.; Hide, F.; Gupta, R.; Miller, E. K.; Moses, D.; Heeger, A. J. *App. Phys. Lett.* **1998**, *72*, 1536–1538.
(10) Mitchell, P. *Nature* **1961**, *191*, 144–148.
(11) Mulkidjaniana, A. Y.; Heberlec, J.; Cherepanove, D. A. *Biochim. Biophys. Acta* **2006**, *1757*, 913–930.
(12) Berridge, M. J.; Lipp, P.; Bootman, M. D. *Nat. Rev. Mol. Cell Biol.* **2000**, *1*, 11–21.
(13) Lee, J.; Panzer, M. J.; He, Y.; Lodge, T. P.; Frisbie, C. D. *J. Am. Chem. Soc.* **2007**, *129*, 4532–4533.
(14) Panzer, M. J.; Frisbee, C. D. *J. Am. Chem. Soc.* **2007**, *129*, 6599–6607.
(15) O'Regan, B.; Grätzel, M. *Nature* **1991**, *353*, 737–740.
(16) Hagfeldt, A.; Grätzel, M. *Acc. Chem. Res.* **2000**, *33*, 269–277.
(17) Snaith, H. J.; Grätzel, M. *Appl. Phys. Lett.* **2006**, *89*, 262114.
(18) Pei, Q.; Yu, G.; Zhang, C.; Yang, Y.; Heeger, A. J. *Science* **1995**, *269*, 1086–1088.
(19) deMello, J. C.; Tessler, N.; Graham, S. C.; Friend, R. H. *Phys. Rev. B* **1998**, *57*, 12951–19962.

LEDs.[18−27] In the latter case, efficient polymer light emitting devices have been fabricated by blending the active layer with electrolytes,[18,19] or substituting it with single-component conjugated polyelectrolytes (CPEs) that have ion pairs tethered to the side chains.[21−24] The added ions were originally believed to facilitate electrochemical doping under applied bias;[18] however, mounting experimental evidence supports an electrodynamic model whereby the redistribution of mobile ions enhances the field locally at the electrodes,[19,28−31] leading to facile and balanced electronic carrier injection. However, solid-state photoluminescence (PL) efficiencies of CPEs are found to be considerably lower than their neutral counterparts[23,24] and dependent on the nature and size of counterions present.[32] Accordingly, CPEs are deployed most effectively as thin injection layers between the electrodes and highly emissive neutral conjugated polymers.[25−27] Extrinsic In^{3+} and Cl^- ions have also been found to induce PL quenching in films of neutral polymers without evidence of any electrochemical doping.[33]

Further exploitation of ions in polymer optoelectronic devices will be enabled by better understanding the interactions between ions and electronic excitations, particularly the origin of the observed luminescence quenching. The difficulty of uncovering the inherent photophysical interactions arises, in part, because ions tethered to conjugated polymers introduce amphiphilic character which can induce rigid ordered backbone conformations and the formation of aggregates and interchain states.[34−36] This prompted us to investigate the solid state photophysics of a derivative of F8BT (poly(9,9′-dioctylfluorene-*alt*-benzothiadiazole)) with a low density of ions that are tethered statistically. This arrangement was chosen to minimize the likelihood of ion-induced ordering while ensuring that ions are distributed with sufficient density to interact with electronic excitations in the film. F8BT is a highly emissive semiconducting polymer that is used as the active layer in efficient LEDs,[37,38] optically pumped lasers,[39] and PV diodes.[40,41] By time resolving emission and absorption spectra of excitons encountering ions in our CPE films, we show that, contrary to existing views, ions do not destroy optical excitations but rather induce the formation of long-lived, weakly emissive and immobile charge-transfer (CT) states via Coulombic interactions.

Experimental Section

Materials. 9,9-Dioctylfluorene-2,7-diboronic acid bis(1,3-propanediol) ester and 2,7-Dibromo-2,1,3-benzothiadiazole were purchased from Aldrich. 2,7-Bis[9,9′-bis(6″-bromohexyl)-fluorenyl]-4,4,5,5-tetramethyl-(1,3,2)dioxaborolane was synthesized according to the literature.[42] The polymerization is based on standard palladium-mediated Suzuki cross-coupling copolymerization of 2,7-bis[9,9-bis(6-bromohexyl)-fluorenyl]-4,4,5,5-tetramethyl-[1.3.2]dioxaborolane (**M1**), 9,9-Dioctylfluorene-2,7-diboronic acid bis(1,3-propanediol) ester (**M2**), and 4,7-dibromo-2,1,3-benzothiadiazole.[43] F8BT and PFB were supplied by Cambridge Display Technology Ltd. Thin films were spin-coated on carefully cleaned spectrosil substrates at a spin speed of 2000 rpm for 60 s from 10 g/L chloroform solutions of the polymers.

Spectroscopy. UV−visible absorption spectra were measured with a Hewlett-Packard 8453 UV−visible system. Steady-state room-temperature PL measurements on dilute solutions and thin films were undertaken using a Varian Cary Eclipse Fluorescence spectrometer with an excitation and emission monochromator. Temperature-dependent PL measurements were carried out using a PicoQuant 470 nm pulsed diode laser (LDH-P-C-470, 100 ps pulse length) as an excitation source (40 MHz repetition rate), and a PI Acton SpectraPro 2500i 0.5 m imaging spectrograph (150 gr/mm grating) coupled to a cooled CCD camera (PI Acton). Samples were contained in an Oxford Instruments Optistat continuous flow He cryostat coupled to a gas flow controller and a temperature controller/heater (ITC502S).

Time-resolved PL measurements were made using the same PicoQuant 470-nm pulsed diode laser as an excitation source at a repetition rate of 20 MHz. A time-correlated single photon counting instrument (Edinburgh Instruments, Lifespec-ps) equipped with an emission monochromator and a Hamamatsu multichannel plate photomultiplier tube detector was used to spectrally and temporally resolve the PL. Samples were contained in a vacuum chamber ($\sim 10^{-5}$ mbar) during TCSPC measurements.

The setup for TA spectroscopy has been described elsewhere.[44] A 1-kHz train of 60 fs pulses (800 μJ/pulse, $\lambda_0 = 800$ nm) is generated in a Ti:Sapphire amplifier system (Spectra-Physics, Spitfire-Pro) that is pumped by a 20-W DPSS Q-switched Nd:YLF laser (Spectra-Physics, Evolution) and seeded by a mode-locked oscillator (Spectra-Physics, Tsunami) with a Millenia-Pro 5-W DPSS laser. A portion of the amplifier output is used to pump a TOPAS optical parametric amplifier, which is used to tune the excitation pulses in the measurements presented here. A further portion of the amplifier output is used to pump a home-built broadband noncollinear optical parametric amplifier (NOPA) that

(20) Bernards, D. A.; Flores-Torres, S.; Abruña, H. D.; Malliaras, G. G. *Science* **2006**, *313*, 1416–1419.
(21) Edman, L.; Pauchard, M.; Liu, B.; Bazan, G.; Moses, D.; Heeger, A. J. *Appl. Phys. Lett.* **2003**, *82*, 3961–3963.
(22) Edman, L.; Liu, B.; Vehse, M.; Swenson, J.; Bazan, G.; Heeger, A. J. *J. Appl. Phys.* **2005**, *98*, 044502.
(23) Huang, F.; Hou, L.; Wu, H.; Wang, X; Shen, H.; Cao, W.; Yang, W.; Cao, Y. *J. Am. Chem. Soc.* **2004**, *126*, 9845–9853.
(24) Huang, F.; Wu, H.; Wang, D.; Yang, W.; Cao, Y. *Chem. Mater.* **2004**, *16*, 708–716.
(25) Wu, H. B.; Huang, F.; Mo, Y. Q.; Yang, W.; Wang, D. L.; Peng, J. B.; Cao, Y. *Adv. Mater.* **2004**, *16*, 1826–1830.
(26) Hoven, C.; Yang, R.; Garcia, A.; Heeger, A. J.; Nguyen, T.-Q.; Bazan, G. C. *J. Am. Chem. Soc.* **2007**, *129*, 10976–10977.
(27) Hoven, C. V.; Garcia, A.; Bazan, G. C.; Nguyen, T.-C. *Adv. Mater.* **2008**, *20*, 3793–3810.
(28) deMello, J. C.; Halls, J. J. M.; Graham, S. C.; Tessler, N.; Friend, R. H. *Phys. Rev. Lett.* **2000**, *85*, 421–424.
(29) Slinker, J. D.; DeFranco, J. A.; Jaquith, M. J.; Silveira, W. J.; Zhong, Y.-W.; Moran-Mirabal, J. M.; Craighead, H. G; Abruña, H; Marohn, J. A.; Malliaras, G. G *Nat. Mater.* **2007**, *6*, 894–899.
(30) deMello, J. C. *Nat. Mater.* **2007**, *6*, 796–797.
(31) Pingree, L. S. C.; Rodovsky, D. B.; Coffey, D. C.; Bartholomew, G. P.; Ginger, D. S. *J. Am. Chem. Soc.* **2007**, *129*, 15903–15910.
(32) Yang, R.; Garcia, A.; Korystov, D.; Mikhailovsky, A.; Bazan, G. C.; Nguyen, T.-Q. *J. Am. Chem. Soc.* **2006**, *128*, 16532–16539.
(33) Morgado, J.; Thomas, D. S.; Friend, R. H.; Cacialli, F *Synth. Met.* **2000**, *111−112*, 549–552.
(34) Nguyen, T.-Q.; Schwartz, B. J. *J. Chem. Phys.* **2002**, *116*, 8198–8208.
(35) Wang, D.; Moses, D.; Bazan, G. C.; Heeger, A. J.; Lal, J. J. *Macromol. Sci.-Pure Appl. Chem.* **2001**, *A38*, 1175–1189.
(36) Al Attar, H. A.; Monkman, A. P. *J. Phys. Chem. B* **2007**, *111*, 12418–12426.
(37) He, Y.; Gong, S.; Hattori, R.; Kanicki, J. *Appl. Phys. Lett.* **1999**, *74*, 2265–2267.
(38) Morteani, A. C.; Dhoot, A. S.; Kim, J.-S.; Silva, C.; Greenham, N. C.; Murphy, C. E.; Moons, E.; Cina, S.; Burroughes, J. H.; Friend, R. H. *Adv. Mater.* **2003**, *15*, 1708–1712.
(39) Xia, R.; Heliotis, G.; Stavrinou, P. N.; Bradley, D. D. C. *Appl. Phys. Lett.* **2005**, *87*, 031104.
(40) Halls, J. J. M.; Arias, A. C.; MacKenzie, J. D.; Wu, W.; Inbasekaran, M.; Woo, E. P.; Friend, R. H. *Adv. Mater.* **2000**, *12*, 498–502.
(41) Snaith, H. J.; Arias, A. C.; Morteani, A. C.; Silva, C.; Friend, R. H. *Nano Lett.* **2002**, *2*, 1353–1357.
(42) Liu, B.; Bazan, G. C. *J. Am. Chem. Soc.* **2006**, *128*, 1188–1196.
(43) Stork, M. S.; Gaylord, B. S.; Heeger, A. J.; Bazan, G. C *Adv. Mater.* **2002**, *14*, 361–366.
(44) Westenhoff, S; Howard, I. A.; Hodgkiss, J. M.; Kirov, K. R.; Bronstein, H. A.; Williams, C. K.; Greenham, N. C.; Friend, R. H. *J. Am. Chem. Soc.* **2008**, *130*, 13653–13658.

Scheme 1

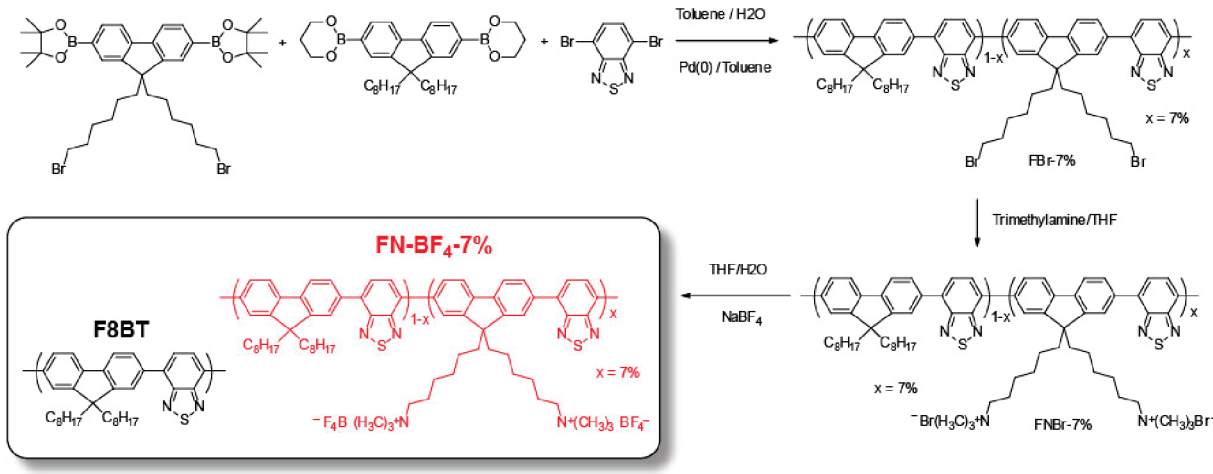

has been described elsewhere.[45] The stable 500−800 nm output of the NOPA is used as a probe (except in the GS recovery experiment, where either the NOPA is tuned to a narrower probe spectrum at 480−500 nm, or the 490 nm TOPAS output is used as both the excitation and probe). The probe beam is delayed relative to the excitation beam via a computer-controlled Newport mechanical delay stage. Half of the probe beam is focused to overlap nearly collinearly with the excitation beam in the sample (with the polarization set to the magic angle of 54.7° to avoid orientational dynamics), while the other half does not overlap with the excitation beam and is used as a reference to normalize minor fluctuations in the probe intensity. The pump and probe beams have fwhm diameters of 400 and 250 μm, respectively, in the plane of the sample. The residual excitation is blocked having passed through the sample. Both the probe and reference beams enter an imaging double-grating spectrograph in the same vertical plane (PI Acton Spectrapro 2150i) and are spectrally dispersed onto two 256 pixel photodiode arrays (Hamamatsu S3901256Q), such that the wavelength calibration is identical for both the probe and reference channels. The video output is read out with a commercially available circuit (C7844, Hamamatsu), digitized for each laser pulse using a PXI-6122 card (National Instruments), and processed with a National Instruments real-time acquisition computer (NI PXI-1002). The excitation beam is chopped at 500 Hz such that the transmission of alternate probe pulses can be compared to obtain the differential transmission as a result of excitation. Differential transmission spectra are obtained by doing so for each pixel, and temporal dynamics are compiled by collecting spectra for a range of relative probe delay times (typically ~150 points are distributed from −10 to 2000 ps). Typically ~500 laser shots are averaged for each data point, and the entire time range is swept 5−10 times. Group velocity dispersion causes a chirp of ~1.5 ps across the 500−800 nm probe spectrum; however, this effect is corrected for by introducing a wavelength-dependent temporal offset during data processing. After making this correction and a negative time background subtraction, the instrument limited time resolution is ~120 fs, as judged by the signal risetime. For polarization anisotropy measurements, we separated s and p polarizations of the 800-nm probe beam with a cube polarizer and detected the $\Delta T/T$ signals with polarization parallel and perpendicular to the excitation source simultaneously using separate photodiodes in addition to a reference photodiode to reduce shot-to-shot noise. Samples were contained in a vacuum chamber (~10^{-5} mbar) during TA measurements.

Results and Discussion

The polymers examined in this study and the synthesis of FN-BF_4-7% are shown in Scheme 1. The synthesis of FNBr-7% is based on the statistical Suzuki-coupling copolymerization of the bis(6-bromohexyl)-fluorenyl boronic ester **M1** and the 9,9-dioctylfluorene boronic ester **M2** with 4,7-dibromo-2,1,3-benzothiadiazol. NMR analysis of FNBr-7% revealed that a 1:9 **M1/M2** feed ratio gave a copolymer containing 7% of the bis(6-bromohexyl)fluorine and 93% of F8BT repeats. The bromohexyl tails were treated with trimethylamine in THF to give the corresponding trimethylammonium derivatives with bromide counterions (FNBr-7%).[42] The counterions were then exchanged to tetrafluoroborate by dissolving the polymer in a THF and water solution containing an excess of $NaBF_4$. The solvent was then removed under reduced pressure, and the solid washed several times with deionized water to give the resulting polymer (FN-BF_4-7%) in 45% yield. The relatively low density of ionic side chains in FN-BF_4-7% ensures that the polymer is soluble in most of the same solvents used to process F8BT.

Figure 1 (top panel) shows the absorption and emission spectra of dilute choloroform solutions (10 mg/L) of FN-BF_4-7% compared with the nonionic F8BT. The spectral features are virtually identical. Moreover, time-resolved PL decays (not shown) are monoexponential and independent of wavelength, with nearly identical lifetimes for FN-BF_4-7% ($\tau = 2.8$ ns) and F8BT ($\tau = 2.9$ ns). The invariance of the photophysics indicates that the ionic side chains and counterions do not interact with

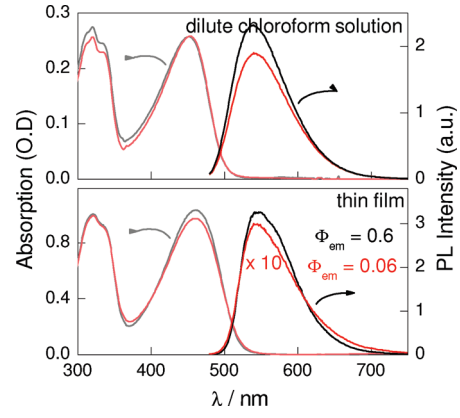

Figure 1. Optical absorption spectra of F8BT (gray) and FN-BF_4-7% (pink) in dilute (10 mg/L) chloroform solutions (top panel) and in thin (~150 nm) films (bottom panel), along with corresponding PL spectra ($\lambda_{exc} = 470$ nm) of F8BT (black) and FN-BF_4-7% (red). PL spectra were measured under identical conditions for F8BT and FN-BF4−7%, ensuring that the relative intensities shown can be compared. For ease of comparison, the PL intensity of the FN-BF_4-7% thin film has been multiplied by a factor of 10.

(45) Laquai, F.; Mishra, A. K; Müllen, K.; Friend, R. H *Adv. Funct. Mater.* **2008**, *18*, 1–11.

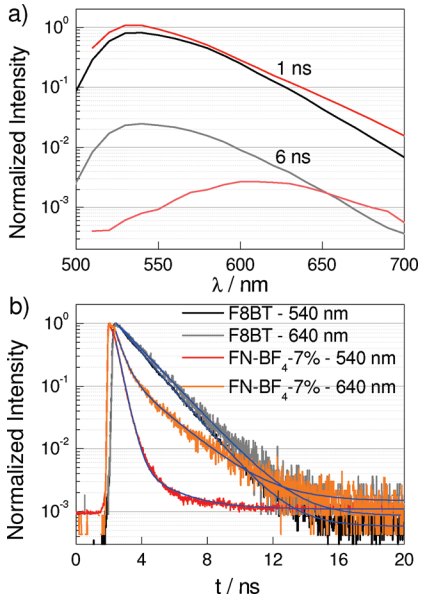

Figure 2. (a) Time-resolved PL spectra of thin films of F8BT (black) and FN-BF4−7% (red) at <1 and 6 ns (gray and pink, respectively) after 470 nm excitation. (b) Time-resolved PL kinetics for F8BT detected at 540 and 640 nm (black and gray, respectively, with monoexponential fits indicated in blue), and for FN-BF4−7% at the same wavelengths (red and orange, respectively, with biexponential fits indicated in blue).

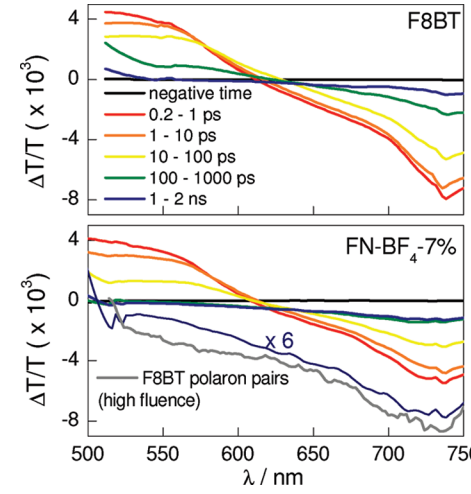

Figure 3. Transient absorption spectra of F8BT (top) and FN-BF_4-7% (bottom) within 2 ns of excitation with integrated time regions indicated (λ_{exc} = 490 nm, fluence <10^{14} photons/cm^2). The 1−2 ns spectrum is duplicated with a magnified scale in FN-BF_4-7% for better comparison with early time spectra. Also shown (gray) is the spectrum of F8BT polaron pairs formed via exciton annihilation under significantly (>25-fold) higher fluence.

the conjugated backbone in dilute solution, nor do they induce aggregation or decomposition. Both effects have been found to lead to PL quenching in solutions of CPEs with exclusively ionic side chains.[34−36]

The bottom panel of Figure 1 shows the absorption and emission spectra of thin films of FN-BF_4-7% and F8BT. Again, the absorption spectra are virtually identical; however, the PL intensity is significantly attenuated for the ionic copolymer FN-BF_4-7% compared with F8BT when measured under identical conditions. The integrated PL quantum efficiency[46] is 6% for FN-BF_4-7% compared with 60% for F8BT.[47] While the PL spectra are all peaked at λ_{em} = 540 nm, comparison of the normalized PL spectra shows that FN-BF_4-7% has slightly enhanced emission on the red tail of the spectrum.

The observation of PL quenching and subtle spectral shifts prompted us to undertake time-resolved measurements by the time-correlated single-photon counting (TCSPC) method in order to better understand the perturbations induced by ions in thin films. Figure 2a shows the time-resolved PL spectra for FN-BF_4-7% (red and pink) compared with F8BT (black and gray). These spectra were obtained by reconstructing kinetic traces taken sequentially at 10-nm intervals throughout the spectrum. The F8BT PL decay kinetics (Figure 2b) are well fit by single exponential functions, with little variation in lifetime across the spectrum (τ(540 nm) = 1.41 ns, R^2 = 0.999; τ(640 nm) = 1.58 ns, R^2 = 0.997), also evident by the invariance of the PL spectra at <1 and 6 ns following excitation. The exciton decay is dominated by radiative relaxation, and the minimal wavelength dependence shows that there is little energetic disorder sampled on the time scale of the measurement. In contrast to this, the FN-BF_4-7% spectra (Figure 2a, red and pink) exhibit strong quenching and a pronounced dynamic redshift. Within the first nanosecond after excitation, the PL spectrum (λ_{max} = 540 nm) closely resembles the excitonic F8BT emission. However, this feature is rapidly quenched (τ = 350 ± 30 ps, approaching the 130-ps instrument response function), largely accounting for the 10-fold reduction in the integrated PL quantum efficiency. A secondary red-shifted emission peak (λ_{max} = 610 nm) is clearly seen on longer time scales (τ = 2.0 ± 0.2 ns). The ions introduced in FN-BF_4-7% have the effect of quenching the primary exciton, while introducing a secondary emissive state that is stabilized by 0.3 eV with respect to the primary exciton. We note that spectral characteristics of the secondary red-shifted emission peak are reminiscent of the emissive interchain[44,48] and intrachain[49,50] CT states formed when F8BT is coupled with electron donors.

We turned to TA spectroscopy as a more direct probe of charge transfer (including nonemissive states), as shown in Figure 3. For reference, the TA spectrum of F8BT (top panel), is characterized by a stimulated emission (SE) feature ($\Delta T/T$ > 0) at wavelengths corresponding to the PL (λ<610 nm), and a photoinduced absorption feature ($\Delta T/T$ < 0) peaked beyond 700 nm that is associated with the red absorption of the exciton.[44,51,52] Aside from the small Stokes shift in the stimulated emission, the decay is broadly wavelength independent and proceeds on the same time scale as GS recovery shown in Figure 6a (we note that the signal is still decaying at the limit of our detection window). This is consistent with the simple decay of mobile emissive excitons to the ground state without the participation

(46) Calculated by integrating plots of $I \times \lambda^4$ vs, $1/\lambda$ for PL spectra taken under identical conditions with 470 nm excitation and normalizing to the absolute PLQE of F8BT measured using the integrating sphere method.[47]

(47) Xia, R; George Heliotis, G; Yanbing Hou, Y; Donal, D. C.; Bradley, D. D. C *Org. Elec.* **2003**, *4*, 165–177.

(48) Huang, Y.-S.; Westenhoff, S.; Avilov, I.; Sreearunothai, P.; Deleener, C.; Hodgkiss, J. M.; Friend, R. H.; Beljonne, D. *Nat. Mater.* **2008**, *7*, 483–489.

(49) Kim, J.-S.; Lu, L.; Sreearunothai, P.; Seeley, A.; Yim, K.-H.; Petrozza, A.; Murphy, C. E.; Beljonne, D.; Cornil, J.; Friend, R. H. *J. Am. Chem. Soc.* **2008**, *130*, 13120–13131.

(50) Petrozza, A. Ph.D. Thesis, Univeristy of Cambridge, 2008.

(51) Westenhoff, S.; Howard, I. A.; Friend, R. H. *Phys. Rev. Lett.* **2008**, *101*, 016102.

(52) Stevens, M. A.; Silva, C.; Russell, D. M.; Friend, R. H. *Phys. Rev. B* **2001**, *63*, 165213.

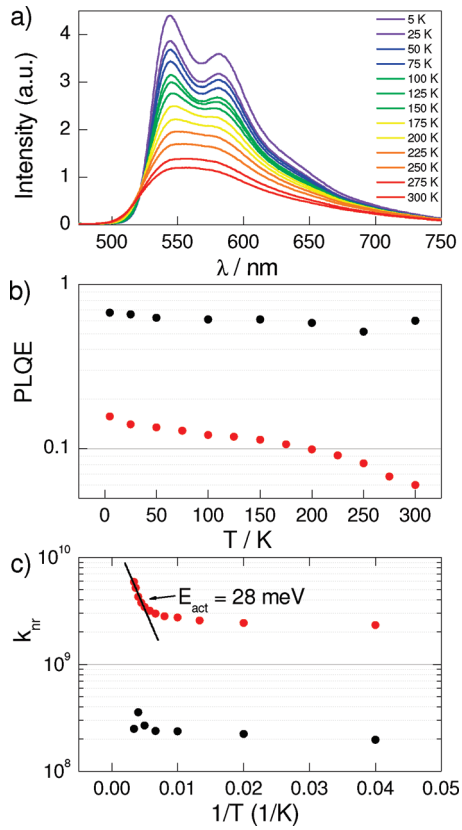

Figure 4. (a) Temperature-dependent PL spectra of FN-BF_4-7%. (λ_{exc} = 470 nm). (b) Temperature-dependent PL quantum efficiency (PLQE) of F8BT (black) and FN-BF_4-7% (red). (c) Arrhenius plot of extracted nonradiative decay rate for F8BT (black) and FN-BF_4-7% (red).

of any other intermediates, as has been shown in previous photophysical studies of F8BT at excitation intensities sufficiently low to avoid charge generation from exciton−exciton annihilation.[51] In the case of FN-BF_4-7% (Figure 3, bottom panel) measured under identical low-fluence conditions, the exciton spectrum 1 ps after excitation (red curve) is virtually identical to that of F8BT, consistent with the conclusion from time-resolved PL that the primary exciton is not affected by the presence of a low density of ions. However, the TA signal of FN-BF_4-7% ceases to evolve after a few hundred picoseconds, and the spectrum of the residual long-lived population (green and blue curves, also duplicated on a magnified scale for better comparison) is characterized by a broadened photoinduced absorption feature peaked beyond 700 nm that extends into the 500−600-nm region where stimulated emission is otherwise expected. These spectral features are consistent with charge photogeneration. For comparison, the TA spectrum of charge pairs in pristine F8BT was independently obtained by exciting the sample with a significantly higher (>25-fold) fluence, known to produce polaron pairs via exciton−exciton annihilation.[52] Indeed, the resulting high-fluence F8BT polaron pair TA spectrum shown in Figure 3 (gray) has a broad visible absorption peaked beyond 700 nm and a lack of SE—strongly reminiscent of the long-lived TA signal measured in FN-BF_4-7% under low fluence (Figure 3, bottom panel). Interchain[38,44,48] and intrachain[49,50] CT states derived from F8BT excitons coupled to electron-donating units have also been shown to give rise to weakened and red-shifted PL, longer radiative lifetimes, loss of SE, and broadened photoinduced absorption across the visible region. The TA and time-resolved PL spectra of FN-BF_4-7%, provide strong evidence that the added ions induce the photogeneration of CT states that have increased electron−hole separation compared with the emissive bound exciton. For brevity, our subsequent references to CT states will include both weakly emissive CT states and nonemissive polaron pairs.

Ionic charges have the potential to stabilize CT states in conjugated polymers by establishing local Coulomb fields that perturb the HOMO and LUMO orbital energies. For example, an anion will raise the energy levels of HOMO and LUMO orbitals of neighboring chains, thus attracting holes and repelling electrons, while a cation will have the reverse effect. The distribution of both anions and cations in the conjugated polymer film is thus expected to lead to local configurations where electron−hole pairs are separated under the influence of ions. The electronic structure of F8BT enhances the interaction with the Coulomb field of ions. The alternating fluorene (donor) and benzothiadiazole (acceptor) units give rise to CT character in the lowest energy excitonic states of F8BT,[53,54] and consequently solvatochromism in the absorption and emission spectra.[50] In solid films of FN-BF_4-7%, CT excitons are expected to be stabilized when BF_4^- counteranions interact with a partially positive fluorene donor unit, whereas destabilization will occur if the BF_4^- ions interact with the partially negative benzothiadiazole (BT) units. Likewise, theoretical calculations show that quarternary amine cations attached to the polymer side chains are poised to undergo electrostatic interaction with electronegative BT units.[55]

Our interpretation of PL quenching is also consistent with recent results from Yang et al.[32] In a series of CPEs derived from F8BT, they report a large increase in PL efficiency (from 5% to 41%) with increasing counteranion size. The authors interpret the trend to arise from decreased interchain interactions when bulkier ions are present, however, we note that Coulombic interactions with excitons will also diminish as the ions are sterically separated from the conjugated backbone.

We can also eliminate several other possible causes of exciton quenching in FN-BF_4-7%. First, the quarternary amine and BF_4^- ions are not redox active toward F8BT in either the GS or the singlet exciton state, thus limiting their role to a physical perturbation upon the polymer photophysics. Second, the absence of heavy atoms precludes the participation of triplet excited states because intersystem crossing operates on a time scale of ∼40 ns in F8BT.[44] Third, the photophysics observed in FN-BF_4-7% is not consistent with the presence of chemical keto defects—fluorenones that are found to appear as photooxidation products in some polyfluorenes.[56,57] Fluorenone defects emit at significantly higher energy ($\lambda_{max} \approx$ 540 nm) than the secondary emissive state we observe in FN-BF_4-7%, and are not considered to be important in fluorene copolymers such as F8BT with lower energy excited states.[58] Additionally,

(53) Cornil, J.; Gueli, I.; Dkhissi, A.; Sancho-Garcia, J. C.; Hennebicq, E.; Calbert, J. P.; Lemaur, V.; Beljonne, D.; Bredas, J. L. *J. Chem. Phys.* **2003**, *118*, 6615–6623.
(54) Jespersen, K. G.; Beenken, W. J. D.; Zaushitsyn, Y.; Yartsev, A.; Andersson, M.; Pullerits, T.; Sundström, V. *J. Chem. Phys.* **2004**, *121*, 12613–12617.
(55) Sheng, Y.; Leszczynski, J.; Nguyen, T.-Q.; Bamgbelu, A. *Struct, Chem.* **2007**, *18*, 827–832.
(56) Scherf, U.; List, E. J. W. *Adv. Mater.* **2002**, *14*, 477–487.
(57) Lupton, J. M.; Craig, M. R.; Meijer, E. W. *Appl. Phys. Lett.* **2002**, *80*, 4489–4491.
(58) Lammi, R. K.; Barbara, P. F. *Photochem. Photobiol. Sci.* **2005**, *4*, 95–99.

spectroscopic measurements on solid films were carried out under vacuum ($<10^{-5}$ Torr) to avoid the possibility of photo-oxidation.

Next we consider the possibility that tethered ions could induce conformational changes to the conjugated backbone, perhaps forming interchain aggregate states that act as recombination sites. Schwartz and co-workers have demonstrated that aggregates form when chains adopt extended conformations that permit close interchain contact; thus, their formation depends strongly upon the nature of polymer side chains and the solvent used for casting films.[59] Aggregates display red-shifted absorption and emission spectra.[59] As previously noted, the low density of tethered ions in FN-BF_4-7% and their statistical incorporation are not expected to cause significant ordering as it can in amphiphilic block copolymers or CPEs with ions attached to all side chains.[35] The invariance of GS absorption spectra and transient absorption polarization anisotropy decay strongly suggest that FN-BF_4-7% retains the same film morphology as F8BT. Additionally, previous studies that directly create and interrogate interchain interactions in F8BT provide little evidence that it could account for the photophysics observed in FN-BF_4-7%.[60,61] Donley et al. used Raman spectroscopy to show that thermal annealing increased the planarity of F8BT and changed the interchain packing from an eclipsed to an alternating packing structure with respect to F8 and BT units of adjacent chains.[61] Thermal annealing induced clear shifts in absorption and PL spectra, yet the corresponding ~10% variation in PL efficiencies shows that such changes in conformation and chain packing are insufficient to explain the strong quenching we observe in FN-BF_4-7%. Schmidtke et al. probed interchain interactions by carrying out photophysical studies on F8BT films under high pressures.[60] Red-shifted absorption and PL spectra at pressures up to 5 GPa were actually explained mostly by the intramolecular planarization of F8BT chains, showing that even highly compressed chain conformations do not represent the photophysics of FN-BF_4-7%.

A low density of ions could not induce such a pronounced perturbation of exciton decay without invoking exciton migration toward ionic sites. This mechanism is exploited for the amplification of exciton quenching via charge- or energy-transfer in sensors,[42,43,62] since excitons diffuse in three dimensions to sample a relatively large volume for the presence of an analyte. In FN-BF_4-7%, two ion pairs are attached to the alkyl side chains of 7% of monomer units in a statistical fashion, and the volume occupied by each monomer unit in a film is estimated to be ~1.3 nm^3 (based on the unit cell reported for F8BT films using X-ray diffraction techniques).[61] Therefore, one would expect the mean distance between neighboring ion pairs to be ~2.7 nm if the ion pairs are randomly dispersed throughout the film, which is certainly within the exciton diffusion radius of F8BT (>10 nm).[51,63] Phase segregation between ionic and nonionic regions could increase the size of pristine nonionic regions; however, the scope for phase segregation is expected to be rather constrained for a statistical copolymer with 7% ionic side chains.

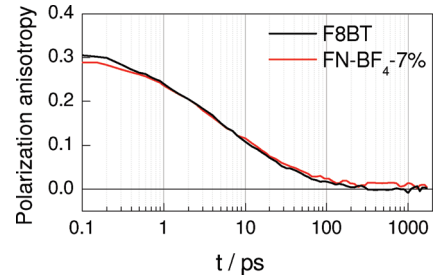

Figure 5. Transient absorption polarization anisotropy kinetics ($\lambda_{exc} = 490$ nm, fluence $<10^{14}$ photons/cm^2, $\lambda_{probe} = 800$ nm) for F8BT (black) and FN-BF4−7% (red). Polarization anisotropy is calculated as $r = (\Delta T/T^{para} - \Delta T/T^{perp})/(\Delta T/T^{para} + 2\Delta T/T^{perp})$.

We undertook low temperature PL measurements in order to investigate the photophysical influence of dispersed ionic sites when exciton diffusion lengths are constrained due to insufficient energy for thermally activated exciton hopping.[64] Figure 4a shows the temperature dependence of PL in FN-BF_4-7%. In addition to the predicted sharpening of vibronic peaks, the PL intensity clearly undergoes a substantial increase with decreasing temperature; the integrated PLQE of FN-BF_4-7% increases nearly ~3-fold upon lowering the temperature from 300 to 5 K, whereas F8BT only exhibits a 1.1-fold increase in PLQE over this range (Figure 4b), along with vibronic peak sharpening. Figure 4c reformulates the PLQE data as an Arrhenius plot in order to examine the activation energy associated with exciton trapping. In this plot, it is assumed that nonradiative relaxation channels account for most of the variation in PLQE; thus, k_{nr} is extracted from each temperature in the series assuming that the radiative lifetime is equal for the two materials and independent of temperature (2.7 ns, based on the measured room temperature PLQE and lifetime of F8BT). While k_{nr} is rather insensitive to temperature for F8BT, the ionic copolymer exhibits two distinct temperature regimes for variation in k_{nr}, corresponding to activation energies of 28 ± 4 (when fitting the range 200−300 K) and 0.1 ± 0.03 meV (when fitting $T < 100$ K). We do not attach any physical significance to the low energy component since it is lower than thermal energy and likely to be susceptible to our assumption about the invariance of k_r. The 28-meV component accounts for most of the observed temperature variation of the PL intensity in FN-BF_4-7%, and we attribute this to the exciton hopping activation energy. The measured activation energy lies within the wide range of reported values, e.g., 170 meV for singlet exciton hopping in PPV,[65] 60 meV for triplet exciton hopping in a Platinum poly yne,[66] and 7 meV for triplet exciton hopping in an Ir(PPy)-cored dendrimer.[67] In these examples, the activation energy for exciton motion is noted to be very sensitive to the nature and strength of intermolecular interactions and the energetic disorder. The variable temperature measurements do not reveal the activation energy for exciton hopping in pristine F8BT due to the absence of quenching sites. Even at low temperature, the PLQE is considerably (~3.5-fold) lower for FN-BF_4-7% than for nonionic F8BT, indicating that exciton diffusion is not completely shut off at low temperature.

(59) Schwartz, B. J. *Annu. Rev. Phys. Chem.* **2003**, *54*, 141–172.
(60) Schmidtke, J. P.; Kim, J.-S.; Gierschner, J.; Silva, C.; Friend, R. H. *Phys. Rev. Lett.* **2007**, *99*, 167401.
(61) Donley, C. L.; Zaumseil, J.; Andreasen, J. W.; Nielsen, M. M.; Sirringhaus, H.; Friend, R. H.; Kim, J.-S. *J. Am. Chem. Soc.* **2005**, *127*, 12890–12899.
(62) McQuade, D. T; Pullen, A. E.; Swager, T. M. *Chem. Rev.* **2000**, *100*, 2537–2574.
(63) Kim, J,-S.; Friend, R. H.; Grizzi, I.; Burroughs, J. H *Appl. Phys. Lett.* **2005**, *87*, 023506.
(64) Mikhnenko, O. V.; Cordella, F.; Sieval, A. B.; Hummelen, J. C.; Blom, P. W. M.; Loi, M. A. *J. Phys. Chem.* **2008**, *112*, 11601–11604.
(65) Bjorklund, T. G.; Lim, S.-H.; Bardeen, C. J. *J. Phys. Chem. B* **2001**, *105*, 11970–11977.
(66) Sudha Devi, L.; Al-Suti, M. K.; Dosche, C.; Khan, M. S.; Friend, R. H.; Köhler, A. *Phys. Rev. B* **2008**, *78*, 045210.
(67) Ribierre, J. C.; Ruseckas, A.; Samuel, I. D. W.; Staton, S. V.; Burn, P. L. *Phys. Rev. B* **2008**, *77*, 085211.

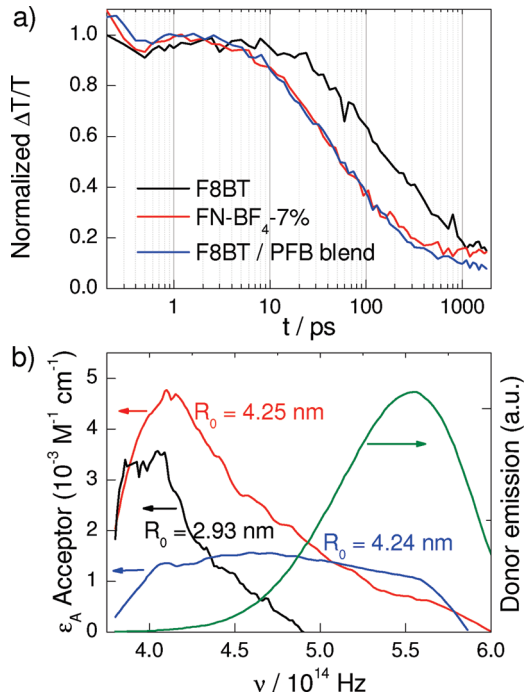

Figure 6. (a) Normalized GS recovery kinetics for F8BT (black), FN-BF_4-7% (red) and an F8BT/PFB blend (blue) (λ_{exc} = 490 nm, fluence = 6 × 10^{13} photons/cm^2, λ_{probe} = 490 nm). (b) Relevant spectra to assess Förster transfer from an F8BT exciton donor (green PL spectrum) to the following acceptors (with absorption shown in units of molar extinction coefficient); an F8BT exciton (black), an FN-BF_4-7% charge pair (red), and an F8BT/PFB charge pair (blue).

Simple geometric considerations suggest that the exciton diffusion radius of FN-BF_4-7% decreases by a factor of 1.44 in going from 300 to 5 K.[68] This is consistent with the ~1.5-fold contraction of the exciton diffusion radius reported for MEH-PPV at low temperature, where a temperature-independent exciton transfer regime persists.[64]

Polarization anisotropy dynamics are a powerful probe of exciton motion in disordered chromophore materials.[44,48,59,69,70] Figure 5 shows polarization resolved transient absorption (TA) kinetics for FN-BF_4-7% (red curve) compared with F8BT (black curve) probed in the photoinduced absorption region at 800 nm (vide infra). The polarization anisotropy decays with a time constant of ~8 ps in both materials, which corresponds to depolarization of excitons in just a few hops—significantly shorter than the time scale of exciton population decay (vide infra). The similarity of polarization anisotropy decays indicates that the ionic subsituents do not significantly alter the film morphology in FN-BF_4-7% compared with F8BT. Additionally, the initial polarization anisotropy levels ($r \approx 0.3$) are sufficiently high to suggest that there is negligible absorption into interchain aggregate states, which has been demonstrated to cause depolarization on an ultrafast time scale.[69] However, the polarization anisotropy does not quite decay to a zero baseline in FN-BF_4-7% as it does in F8BT. The nonzero anisotropy baseline corresponds to the residual population of long-lived excitations in the ionic copolymer, leading us to conclude that the residual population is immobile. The small magnitude of long-lived anisotropy is simply a consequence of rapid depolarization during the exciton hopping steps prior to trapping, thus only the fraction of excitons that were trapped in CT states within the first few hops are expected to retain polarization anisotropy.

Finally, we sought to quantify the fraction of excitations that form long-lived CT states (rather than decaying to the GS) by measuring the GS recovery kinetics at a wavelength (λ_{probe} = 490 nm) that is resonant with the GS absorption band and too high in energy to induce excited state absorption or stimulated emission. Figure 6a shows the normalized kinetics of GS recovery for FN-BF_4-7% and F8BT. Low excitation fluences (6 × 10^{13} ph/cm^2) were used to preclude the effect of exciton−exciton interactions. When considering the first 400 ps of the kinetics trace, the ionic copolymer undergoes significantly faster GS recovery compared with F8BT. Beyond this time, a residual signal is retained out to the maximum time delay of 1.7 ns, whereas the F8BT continues to proceed toward complete GS recovery. The residual signal in FN-BF_4-7% corresponds to ~15% of the initial excited state population. This result appears to imply that the presence of ions primarily accelerates the decay of most excitons to the ground state nonradiatively, with only small residual (<15%) trapped as CT states to contribute to the red-shifted emission and transient absorption signal. However, we see no plausible mechanism that could readily account for such rapid nonradiative decay of excitons, as required to reconcile the picosecond GS recovery kinetics with the low steady-state PLQE in the presence of redox-inert ions.

Instead, we consider whether excitons could be quenched by prior photogenerated charges at the excitation intensities used in the TA measurements. Singlet excitons are known to be efficiently quenched by polarons in conjugated organic materials, typically via Förster resonant energy transfer from an emissive exciton to an absorbing polaron.[71−76] The enhanced visible absorption of charges relative to excitons means that this bimolecular decay channel can still be operative at excitation densities below the threshold of exciton−exciton annhiliation. We calculated the Förster radius for resonant energy transfer from an F8BT exciton to an absorbing CT state. According to the application of Förster theory to conjugated polymers, the Förster radius (R_0) is given by[77−79]

$$R_0^6 = \frac{9000(\ln 10)\kappa^2}{128\pi^5\eta^4 N_{Av}} c^4 \int_0^\infty \frac{f_D(\nu)\varepsilon_A(\nu)}{\nu^4}\, d\nu \qquad (1)$$

In eq 1, κ^2 is the orientational factor (taken to be 0.655 for the case where the donor and acceptor dipoles lie in the plane of the film),[52] η is the refractive index of the medium (previously measured to be 1.8 by ellipsometry),[52] N_{Av} is Avogadro's

(68) Assuming that the 3-fold increase in PLQE for FN-BF_4-7% at low temperature corresponds to a 3-fold decrease in the exciton diffusion volume, the exciton diffusion radius is reduced by $\sqrt[3]{3}$.

(69) Chang, M. H.; Frampton, M. J.; Anderson, H. L.; Herz, L. M. *Phys. Rev. Lett.* **2007**, *98*, 027402.
(70) Nguyen, T.-Q.; Wu, J.; Doan, V.; Schwartz, B. J.; Tolbert, S. H. *Science* **2000**, *288*, 652–656.
(71) Bradley, D. D. C.; Friend, R. H. *J. Phys.: Condens. Matter* **1989**, *1*, 3671–3678.
(72) Dyakonova, V.; Frankevich, E. *Chem. Phys.* **1998**, *227*, 203–217.
(73) McNeill, J. D.; Barbara, P. F. *J. Phys. Chem. B* **2002**, *106*, 4632–4639.
(74) Baldo, M. A.; Holmes, R. J.; Forrest, S. R. *Phys. Rev. B.* **2002**, *66*, 035321.
(75) Graupner, W.; Partee, J.; Shinar, J.; Leising, G.; Scherf, U. *Phys. Rev. Lett.* **1996**, *77*, 2033–2036.
(76) List, E. J. W.; Kim, C.-H.; Naik, A. K.; Scherf, U.; Leising, G.; Graupner, W.; Shinar, J. *Phys. Rev. B* **2001**, *64*, 155204.
(77) Förster, T. *Ann. Phys. (Leipzig)* **1948**, *2*, 55–75.
(78) Förster, T *Discuss. Faraday Soc.* **1959**, *27*, 7–17.
(79) Duysens, L. N. M. *Prog. Biophys. Mol. Biol.* **1964**, *14*, 1–104.

number, $f_D(\nu)$ is the emission spectrum of the donor (in this case an F8BT singlet exciton) normalized such that $\int f_D(\nu)\, d\nu = 1$, and $\varepsilon_A(\nu)$ is the absorption spectrum of the acceptor (the CT state in this case) in units of molar extinction coefficient (M^{-1} cm^{-1}). The absorption spectrum is obtained in the appropriate units using

$$\varepsilon(\nu) = \frac{\log_{10} e}{1000} N_{Av} \sigma(\nu) \quad (2)$$

where $\sigma(\nu)$ is the absorption cross-section calculated from the transient transmission spectrum using

$$\sigma(\nu) = -\frac{1}{Nz} \ln\left(1 + \frac{\Delta T}{T}(\nu)\right) \quad (3)$$

In eq 3, the excitation density ($N = 4.7 \times 10^{17}$ cm^{-3}) is determined from the product of the incident fluence (6×10^{13} ph/cm^2), the absorption efficiency at the excitation wavelength ($\eta_{490nm} = 0.78$), the fraction of excitions that survive beyond 1 ns where the spectrum is measured ($\Phi = 0.15$, based in the red curve in Figure 6a), and the film thickness ($z = 150$ nm). A strong Förster overlap for quenching by CT states (red curve) is evident in Figure 6b, corresponding to a Förster radius of 4.25 nm. This is considerably higher than the corresponding radius for quenching by another F8BT exciton (2.93 nm, black curve),[80] corresponding to a 10-fold enhancement in the Förster transfer rate when the ratio is taken to the sixth power according to the Förster equation. It is clear from Figure 6b that the loss of SE and the extension of absorption into the PL region accounts for the enhanced Förster quenching by CT states. At the excitation densities employed for the TA studies, the mean distance between initial excitations ($r = \sqrt[3]{(1/N_0)} = 6.9$ nm approaches the calculated Förster radius, indicating that photogenerated CT states in FN-BF_4-7% are indeed likely to rapidly quench nearby excitons at the fluences used. We note that comparing the Förster radius to the mean distance between excitations is overly simplistic for many reasons, including (i) the distribution of excitations is neither uniform nor static on the time scale of quenching (as demonstrated by the temperature dependent PL and the 8-ps exciton depolarization), (ii) an exciton can undergo multiple pairwise interactions with quenching sites in a film, resulting in a cumulative quenching rate, (iii) the point-dipole model that underpins Förster theory breaks down for the closely packed arrays of elongated chromophores encountered in conjugated polymers,[81] and (iv) additional (nonresonant) mechanisms could also contribute to charge-induced exciton quenching. Taking these corrections into account will enhance the predicted rate of exciton quenching by CT states.

Rather than attempting to quantify these corrections, we measured GS recovery kinetics under identical conditions for F8BT blended with PFB (poly(9,9-dioctylfluorene-*co*-bis-*N,N′*-(4,butylphenyl)-bis-*N,N′*-phenyl-1,4-phenylene-diamine), a combination that is known to readily facilitate charge photogeneration and photovoltaic behavior.[38,40,44,48] We were able to prepare a blended film morphology that exhibited F8BT exciton quenching on a comparable time scale to FN-BF_4-7% by casting the film (1:1 F8BT/PFB by weight) from a mixture of low- and high- boiling-point solvents,[82] in this case chloroform/chlorobenzene (90:10 by volume). The conversion of excitons to long-lived charge-pairs is known to be very efficient in this blend under steady state excitation ($\Phi_{exciton \rightarrow charge} > 60\%$).[82,44,48] Therefore, if no additional quenching channels were operational, one would expect the blend to exhibit GS recovery kinetics similar to unblended F8BT, but with the decay arrested at >0.6 of the initial level corresponding to the charge population. However, we observe that the GS recovery kinetics are markedly accelerated in the blend and only <10% of excitations[83] survive 2 ns after the excitation pulse (Figure 6a, blue curve). Figure 6a is taken as strong evidence that excitons are quenched by prior photogenerated charges in both the ionic polymer FN-BF_4-7%, and the donor−acceptor blend at fluences below the threshold for exciton−exciton annihilation. Accordingly, figure 6b shows that the overlap integral for Förster quenching via interfacial charge-pairs in the F8BT/PFB blend ($R_0 = 4.24$ nm) is nearly identical to that of the CT state in FN-BF_4-7% ($R_0 = 4.25$ nm). Exciton quenching by photogenerated charges under pulsed excitation in FN-BF_4-7% causes us to underestimate the fraction of excitons that form CT states under steady state conditions. Comparison with GS recovery kinetics in the donor−acceptor blend implies that under steady state excitation, ions will induce the majority of excitons to convert to CT states in the CPE, potentially accounting for all of the observed PL quenching.

Conclusions

We have synthesized a CPE with a low-density ionic side chains and applied time-resolved spectroscopy techniques in order to isolate the inherent interactions between excitons and ionic charges in CPE films. Time-resolved emission and absorption spectroscopy show that in films of FN-BF_4-7%, the primary exciton resembles that of the nonionic counterpart (F8BT). Excitons then undergo activated hopping ($E_{act} = 28$ meV) until the majority encounter a region where ions interact with the polymer backbone in FN-BF_4-7%. Beyond this time scale, the excited-state population exhibits longer-lived emission that is stabilized by 0.3 eV, loss of stimulated emission, and a broadened photoinduced absorption signal. These spectral features provide strong evidence for photogenerated CT states induced by the interaction of ions with bound excitons in CPEs.

These findings have significant implications for the design of conjugated polymer devices that incorporate ionic charge carriers. Unless the interaction between ions and conjugated polymer backbones is well-controlled, morphologies must be optimized to exclude ions from exciton transporting domains. In the case of LEDs, it is notable that ions are most effectively deployed as a layer that is well-separated from the recombination zone where emissive excitons are generated.[25−27] Producing a favorable morphology that exploits mobile ionic charges to assist electronic charge separation in bulk heterojunction polymer PV devices is more challenging. Here, ions must be distributed on

(80) The initial exciton spectrum (within the first 1 ps) is used and converted to units of molar exctinction coefficient in the same way as for the CT spectrum, but without the need to account for population density decay. Stimulated emission causes the spectrum become negative beyond 4.8×10^{14} Hz (this region is excluded from the Förster overlap integral).

(81) Westenhoff, S.; Daniel, C.; Friend, R. H.; Silva, C.; Sundström, V.; Yartsev, A. *J. Chem. Phys.* **2005**, *122*, 094903.

(82) Campbell, A. R.; Hodgkiss, J. M.; Westenhoff, S.; Howard, I. A.; Marsh, R. A.; McNeill, C. R.; Friend, R. H.; Greenham, N. C. *Nano Lett.* **2008**, *8*, 3942–3947.

(83) We note that this level might be partially suppressed by an overlapping PFB charge absorption.

(84) Chia, P.-J.; Sivaramakrishnan, S.; Zhou, M.; Png, R.-Q.; Chua, L.-L.; Friend, R. H.; Ho, P. K. H. *Phys. Rev. Lett.* **2009**, *102*, 096602.

the nanometer length scale at donor−acceptor interfaces throughout the active layer in order to assist charge separation, while being excluded from within exciton transporting domains. Our data show that excitons are effectively funneled toward ionic regions, opening intriguing possibilities to direct the motion of excitons by controlling the spatial distribution of ions and their interaction strengths. We note that counterions could be readily substituted in order to tune the energetic balance between excitons and separated charges in CPEs. In this fashion, it was recently demonstrated that spectator cations can be substituted in doped organic semiconductors in order to tune the work-function over a wide range.[84]

Acknowledgment. This work was supported by a grant from the U.K. Engineering and Physical Sciences Research Council (EPSRC).

JA902167A